Journal of Materials Chemistry A

RSC Publishing

PAPER

View Article Online
View Journal | View Issue

Novel rGO/α-Fe_2O_3 composite hydrogel: synthesis, characterization and high performance of electromagnetic wave absorption†

Cite this: *J. Mater. Chem. A*, 2013, **1**, 8547

Hui Zhang,[ac] Anjian Xie,[c] Cuiping Wang,[c] Haisheng Wang,[b] Yuhua Shen*[b] and Xingyou Tian*[a]

Received 29th March 2013
Accepted 10th May 2013

DOI: 10.1039/c3ta11278k

www.rsc.org/MaterialsA

A novel 3D composite hydrogel composed of reduced graphene oxide nanosheets and α-Fe_2O_3 nanoparticles (rGO/α-Fe_2O_3) was synthesized *via* a two-step process in a solution phase technique. The experimental results show the composite has an interconnected 3D porous network with micrometer pores, and the α-Fe_2O_3 nanoparticles with the size of about 50–100 nm are uniformly dispersed onto the thin graphene nanosheets. The rGO/α-Fe_2O_3 composite hydrogel exhibits excellent microwave absorbability. Compared to a pristine reduced graphene oxide (rGO) hydrogel, the reported composite hydrogel has both wider and stronger wave absorption achieved in the frequency range of 1–18 GHz. The composite with a coating layer thickness of 5.0 mm exhibits a maximum absorption of −33.5 dB at 7.12 GHz and in particular, the product with a coating layer thickness of only 3.0 mm shows a bandwidth of 6.4 GHz (from a frequency of 10.8–17.2 GHz) corresponding to reflection loss at −10 dB. The excellent microwave absorption properties are ascribed to the improved impedance matching. Our findings pave a way to design and prepare lightweight and high performance electromagnetic wave absorption materials based on 3D graphene and other nanomaterials.

Introduction

Electromagnetic (EM) wave absorbing materials have attracted much attention because of their potential applications in wireless data communication, local area networks, satellite television and self-concealing.[1] Great effort has been made for the development of high performance EM wave absorption materials. Carbon based composite materials show very good EM absorption properties and they have other important technical requirements for effective and practical EM wave absorption applications such as being light-weight, having high complex permittivity values, *etc*.[2–4] Graphene, a new kind of carbon based material, has received significant attention in recent years due to its unique electronic, mechanical, and thermal properties since its discovery in 2004.[5,6] Due to their superior properties, graphene and their composites are used for field effect transistors,[7] supercapacitors,[8,9] lithium ion batteries,[10] gas sensors,[11] chemical sensors,[12] *etc.* Recently, scientists found out that chemically reduced graphene oxide and their composites are believed to exhibit good microwave absorption properties and can be used as wave absorbing materials. Wang *et al.*[13] studied the microwave absorption property of chemically reduced graphene oxide (r-GO) and concluded that the r-GO showed enhanced microwave absorption compared with graphite and CNTs, and high quality graphene due to many defects and chemical groups. The dielectric loss is the main microwave absorbing mechanism of r-GO. Such as it is, the value of microwave absorption is −6.9 dB, not an ideal material in microwave absorption applications. Furthermore, Guan *et al.*[14] synthesized hybrid Fe_3O_4/graphene nanocomposite with an assembled Fe_3O_4 nanoparticle superlattice on both sides of 1 nm graphene and found the composite exhibited both enhanced dielectric losses and magnetic losses at 1–18 GHz. Bi *et al.*[4] prepared a novel kind of bowl-like hollow Fe_3O_4/r-GO composite. The composite exhibited a maximum absorption of −24 dB at 12.9 GHz. In addition to these, researchers have also studied the microwave absorption properties of chemically reduced graphene (CR-G)/poly(ethylene oxide) (PEO) composites,[15] h-Ni/GN and c-Ni/GN hybrid nanomaterials[16] and graphene/polyaniline nanorod arrays.[17] They found that the microwave absorption property would be efficiently enhanced by incorporating these materials into graphene sheets. However, all this research was confined to study the microwave absorption property of two-dimensional (2D) graphene and 2D graphene composites. Macroscopic

[a]*Key Laboratory of Materials Physics, Institute of Solid State Physics, Chinese Academy of Sciences, Hefei, 230031, P. R. China. E-mail: zhhui@ahu.edu.cn; xytian@issp.ac.cn; Fax: +86-0551-5108702; Tel: +86-0551-5108702*

[b]*School of Chemistry and Chemical Engineering, Anhui University, Hefei, 230039, P. R. China. E-mail: s_yuhua@163.com; Fax: +86-0551-5108702; Tel: +86-0551-5108702*

[c]*School of Physics and Materials Science, Anhui University, Hefei, 230039, P. R. China. E-mail: anjx@163.com; Fax: +86-0551-5108702; Tel: +86-0551-5108702*

† Electronic supplementary information (ESI) available. See DOI: 10.1039/c3ta11278k

three-dimensional (3D) graphene structures such as foams, gels, and other networks have recently attracted extensive attention because of the desire to realize practical applications.[9,10,18–22] However up to now, there has been no report on studying the microwave absorption property of 3D graphene and 3D graphene-based composite. Therefore, it is a great challenge to design and prepare good EM absorbing materials based on 3D graphene and other nanomaterials.

Here, a novel two-step process in a solution phase technique for fabrication of macroscopic rGO/α-Fe_2O_3 composite hydrogel with 3D interconnected networks is reported. Although rGO/Fe_2O_3 nanoparticle composites have received great attention in recent years,[23–27] they are used in lithium ion batteries, supercapacitors, *etc.* There are no reports on this composite being used in the EM wave absorption area. Moreover, previous works are focused on Fe_2O_3 nanoparticles anchored on 2D graphene nanosheets. We are first to prepare an rGO/α-Fe_2O_3 composite hydrogel for a 3D porous network structure. Furthermore, previous researchers used Fe^{3+} as the precursor, but we use Fe_3O_4 sol as the precursor because the nanoscale Fe_3O_4 nanoparticles can homogeneously disperse in the GO aqueous suspension and could be easily embedded into the graphene network.[10] During the hydrothermal process, the Fe_3O_4 nanoparticles are oxidised to Fe_2O_3 nanoparticles. As α-Fe_2O_3 nanoparticles are assembled into the 3D framework of graphene, the EM wave absorption properties of the material are significantly enhanced. The enhanced EM wave absorption properties are attributed to better impedance matching of the rGO/α-Fe_2O_3 composite hydrogel. Moreover, the added amount of the composite hydrogel into the paraffin matrix is only 8 wt%. Thus, the rGO/α-Fe_2O_3 composite hydrogel is very promising as a lightweight EM wave absorbing material.

Experimental section

Preparation

Graphite oxide was synthesized from natural graphite powder (325 mesh, Qingdao Huatai Lubricant Sealing S&T Co. Ltd., Qingdao, China) using a modified Hummers' method.[8,28] To prepare suspensions of GO, the graphite oxide was sonicated (KQ 800KDV, Kunshan, China) in water for 1 h to give a brown colloidal solution and then centrifuged (TG16-WS, Changsha, China) at 4000 rpm for 20 min to remove any unexfoliated materials.

rGO/α-Fe_2O_3 composite hydrogel was synthesized by a hydrothermal method with GO and Fe_3O_4 nanoparticles as the raw materials. The Fe_3O_4 nanoparticles were prepared by the references.[10,29] In detail, 5.2 g $FeCl_3$ (32 mmol) and 3.18 g $FeCl_2 \cdot 4H_2O$ (16.0 mmol) were dissolved in 25 mL ultrapure water with 0.86 mL of HCl, and then the mixture was added dropwise into 250 mL of 1.5 M NaOH aqueous solution under vigorous stirring. The black precipitate was obtained by centrifugation at 6000 rpm (3 min), and the precipitation was washed with ultrapure water 3 times. Then, 250 mL of a 0.01 M HCl solution was added to neutralize the anionic charges on the nanoparticles. The cationic Fe_3O_4 nanoparticles were collected by centrifugation at 10 000 rpm (10 min) and then freeze dried. The mixture containing 2 mg mL^{-1} GO and different concentrations of Fe_3O_4 nanoparticles was sealed in a 20 mL Teflon-lined autoclave and maintained at 180 °C for 12 h. Three composites with the weight ratios of the raw material as GO to Fe_3O_4 nanoparticles, 4 : 5 (sample-1), 2 : 5 (sample-2) and 1 : 5 (sample-3) were prepared. Then the autoclave was naturally cooled to room temperature and the as-prepared hydrogels were taken out with tweezers. Subsequently, the composite hydrogels were freeze dried under vacuum for further characterization. The corresponding as-synthesized products were named as product-1, product-2 and product-3, respectively. For comparison, the pure rGO hydrogel, α-Fe_2O_3 nanoparticles and 2D rGO/α-Fe_2O_3 composites were fabricated by the same hydrothermal process using 2 mg mL^{-1} GO, 10 mg mL^{-1} Fe_3O_4 solution and the mixture containing 0.3 mg mL^{-1} GO and 0.375 mg mL^{-1} Fe_3O_4 nanoparticles (the weight ratio is the same as sample-1) as the raw materials, respectively. All the reagents used for the experiments were of analytical grade and used directly without further purification. DI water was used in all the processes of aqueous solution preparation and washings.

Characterization

As synthesized Fe_3O_4 nanoparticles and hydrogels were characterized by X-ray diffraction (XRD) using a DX-2700 X-ray Diffractometer equipped with Cu Kα sealed tube ($\lambda = 1.5406$ Å). The samples were scanned in the range between 5° and 80° with a step size of 0.02°. Scanning electron microscopy (SEM) images were performed on a Hitachi SU1510 scanning electron microscope with energy-dispersive X-ray (EDX) analysis (INCA x-ACT). Raman spectroscopy was performed on an inVia-Reflex Raman Microscope equipped with a 532 nm laser in the range of 100–2000 nm. X-Ray photoelectron spectroscopy (XPS) was performed on an ESCALAB-MKII spectrometer (VG Co., UK) with Al Kr X-ray radiation as the X-ray source for excitation. Transmission electron microscopy (TEM) images on a Cu grid were obtained using a JEM 2100 microscope and an accelerating voltage of 100 kV. The thermogravimetric (TG) analysis of the composite hydrogels were performed on a Q2000 thermogravimetric analyzer at a heating rate of 10 °C min^{-1} in air.

Electromagnetic measurements

The electromagnetic parameters of the samples (pure RGO hydrogel, rGO/α-Fe_2O_3 composite hydrogel) were measured in a VNA, AV3629D vector network analyzer in the range of 1–18 GHz after a full two-port calibration (SHORT–OPEN–LOAD–THRU). The measured samples were prepared by uniformly mixing 8 wt% of the sample with a paraffin matrix. The mixture was then pressed into toroidal shaped samples with an outer diameter of 7.00 mm and inner diameter of 3.04 mm.

Results and discussions

The XRD patterns of the pure rGO hydrogel, Fe_3O_4 nanoparticles, and the resulting composites of the rGO/α-Fe_2O_3 composite hydrogels are shown in Fig. 1a. It can be seen that the pure rGO hydrogel shows a very broad diffraction peak at 2θ of

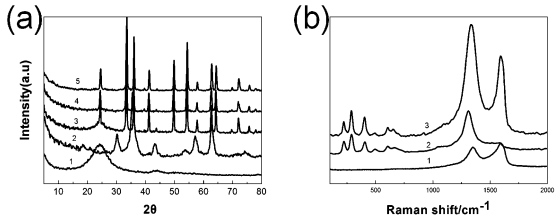

Fig. 1 (a) XRD patterns of the as-synthesized samples (pure rGO hydrogel (1), Fe_3O_4 nanoparticles (2), product-1 (3), product-2 (4) and product-3 (5)), and (b) Raman spectra of the as-synthesized samples (GO (1), α-Fe_2O_3 (2), product-2 (3)).

ca. 25.0°, which means that all of the graphene oxide has been transformed to reduced graphene oxide with significantly less functionalities.[30] Curve 2 is the XRD pattern of the Fe_3O_4 nanoparticles, the series of diffraction peaks at $2\theta = 30.2°$, 35.5°, 43.3°, 53.6°, 57.2°, and 62.9° are assigned to reflections from the (220), (311), (400), (422), (511), and (440) crystal planes (JCPDS no. 01-076-5337). Curves 3, 4 and 5 are the composite hydrogels with fabrication by different weight ratios of GO and Fe_3O_4 nanoparticles, they show similar XRD patterns corresponding to the same hematite phase α-Fe_2O_3 of rhombohedral structure (space group $R\bar{3}c$) (JCPDS no. 01-072-6226). Notably, no obvious diffraction peaks for the pure rGO hydrogel can be observed in the composites of the rGO/α-Fe_2O_3 composite hydrogels, which might be due to the relatively low diffraction intensity of rGO hydrogel in the composites of the rGO/α-Fe_2O_3 composite hydrogels.

The Raman spectra of GO, as-prepared α-Fe_2O_3 nanoparticles and rGO/α-Fe_2O_3 composite hydrogel (product-2) are shown in Fig. 2b. All characteristic bands of α-Fe_2O_3 in the lower wavenumber range exist in the Raman spectrum for the rGO/α-Fe_2O_3 composite hydrogel. But the intense feature at around 1310 cm^{-1} is shifted to 1335 cm^{-1} in the composite. Maybe the band is overlapped by the D band (around 1359 cm^{-1}) in the graphene and formed a new peak at 1335 cm^{-1}. Notably, the bands at about 1593 cm^{-1} (G band) for the graphitized structures are also observed in the composite, which confirms the presence of graphene in the rGO/α-Fe_2O_3 composite hydrogel.

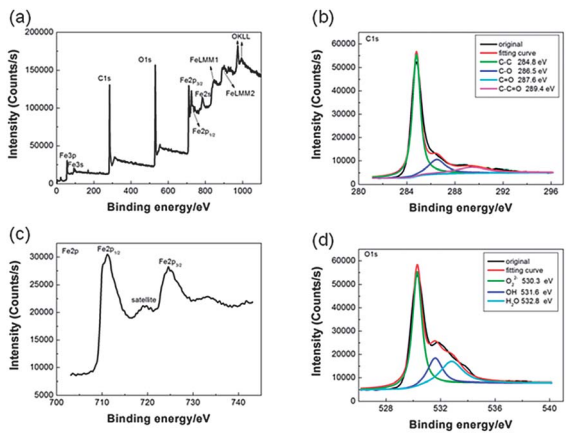

Fig. 2 (a) The general XPS, (b) C 1s region, (c) Fe 2p region and (d) O 1s region for the product-2.

The elemental components of the rGO/α-Fe_2O_3 composite hydrogels is identified by XPS technique. Fig. 2a shows a general XPS profile for rGO/α-Fe_2O_3 composite hydrogel (product-2). The figure reveals that the composite hydrogel is completely composed of Fe, O and C elements. No other elemental signals are detected in the general XPS spectrum. The strong C 1s peak arises from the graphene in the sample. The intensities of all C 1s peaks of the carbon binding to oxygen (Fig. 2b) are very weak indicating that the GO is reduced. The core level binding energy at 711.2 and 724.6 eV are the characteristic doublets of Fe $2p_{3/2}$ and $2p_{1/2}$ core-level spectra of Fe_2O_3, respectively, as shown in Fig. 2c. Also, the corresponding satellite peak located at 719 eV can be solely attributed to the presence of Fe^{3+} ions of α-Fe_2O_3.[31,32] The O 1s spectrum (Fig. 2d) with the peak positions at the binding energies of 530.3 eV, 531.6 eV and 532.8 eV are attributed to O 1s of α-Fe_2O_3, OH and H_2O molecules, respectively.[31]

Fig. 3a shows the SEM image of the pure rGO hydrogel. From it, we can see the pure rGO hydrogel has an interconnected three-dimensional porous network with submicrometer and micrometer pores. We also investigate the morphology of the as-prepared Fe_3O_4 nanoparticles by TEM technique, and the size of the nanoparticles is about 10 nm with homogeneous shapes (Fig. 3b). The SEM image of the freeze-dried composite hydrogel (product-2) is displayed in Fig. 3c. Clearly, it is also an

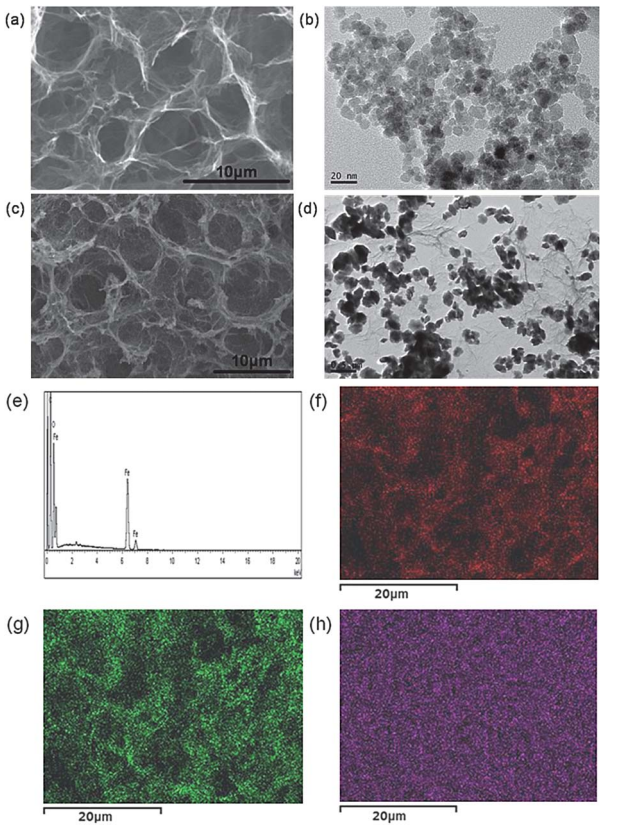

Fig. 3 SEM images of (a) pure rGO hydrogel, (c) product-2; TEM images of (b) Fe_3O_4 nanoparticles, (d) product-2; (e) energy dispersive X-ray (EDX) analysis, EDS mapping of (f) C, (g) O and (h) Fe elements of product-2.

interconnected network with a porous structure, and the pores are micrometers in size. It can be intangibly noted that many nanoparticles decorated the wall of the graphene sheets. Furthermore, the TEM image of Fig. 3d shows that the nanoparticles with a size of about 50–100 nm are anchored onto the thin graphene sheets; no particles that are disassociated from the graphene sheets were observed. In particular, energy dispersive X-ray (EDX) analysis (Fig. 3h) suggests that the three elements C, O and Fe are in the hydrogel. In order to know the dispersion of α-Fe_2O_3 nanoparticles in the 3D graphene framework, we performed elemental mapping analysis of C, O, and Fe (Fig. 3f–h) for the rGO/α-Fe_2O_3 composite hydrogel. They clearly verify the homogeneous α-Fe_2O_3 throughout the 3D macroporous framework. We used TG analysis to clarify the weight ratio of α-Fe_2O_3 nanoparticles in the composite hydrogel, the results are shown in Fig. S1.† The weight loss between 25–100 °C and 200–570 °C can be ascribed to the loss of absorbed water and the pyrolysis of graphene, respectively. From Fig. S1,† we can see the mass loading of α-Fe_2O_3 to the composite hydrogel is about 60 wt%, 76 wt% and 82 wt% in product-1, product-2 and product-3, respectively.

On the basis of the above characterizations and analyses, we propose a possible formation mechanism of rGO/α-Fe_2O_3 composite hydrogel as illustrated in Scheme 1. At the beginning, it was a homogeneous suspension after mixing GO and Fe_3O_4 nanoparticles. During the hydrothermal process, the reduced graphene oxide sheets are self-assembled into the 3D hydrogel with interconnected networks driven by combined hydrophobic and π–π stacking interactions, due to the decrease of oxygenated groups on the graphene.[8,18] Meanwhile, all the Fe_3O_4 nanoparticles homogeneously dispersed in the GO aqueous suspension could be embedded into the graphene network to form a 3D hydrogel.[10] With the oxidation ability of GO, the Fe^{2+} ions in the Fe_3O_4 nanoparticles are oxidized to Fe^{3+} in the formation of α-Fe_2O_3.

We investigated the electromagnetic parameters (complex permittivity and permeability) of the rGO/α-Fe_2O_3 composite hydrogels to reveal their microwave absorbing properties. Fig. 4 shows the real part (ε') and imaginary part (ε'') of the complex permittivity of pure rGO hydrogel and its composites in the frequency range of 1–18 GHz. The ε' and ε'' of pure rGO hydrogel and rGO/α-Fe_2O_3 composite hydrogel decreased with increasing frequency in the 1–18 GHz range, which may be related to a resonance behavior that was reported before.[2,15,33] The composites have much lower ε' and ε'' than the pure rGO hydrogel. And with increasing the content of α-Fe_2O_3, even lower ε' and ε'' are achieved because α-Fe_2O_3 is a kind of semiconductor material, which leads to the conductivity decreasing of the rGO/α-Fe_2O_3 composite hydrogels. According to the free electron theory, low conductivity would result in low permittivity.[13,34,35]

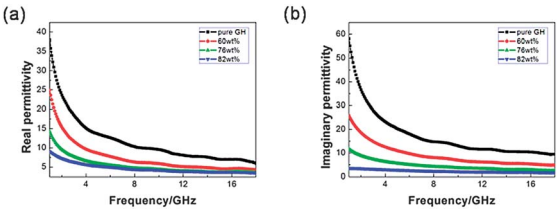

Fig. 4 Electromagnetic characteristics of pure rGO hydrogel and the composite hydrogel with different weight ratios of α-Fe_2O_3 nanoparticles in the 1–18 GHz range: (a) real part of complex permittivity and (b) imaginary part of complex permittivity.

To reveal the microwave absorption properties of the composites, the reflection loss (RL) values are calculated according to the transmission line theory as follows:

$$Z_{in} = Z_0(\mu_r/\varepsilon_r)^{1/2}\tanh[j(2\pi fd/c)(\mu_r\varepsilon_r)^{1/2}] \quad (1)$$

$$RL = 20\log|(Z_{in} - Z_0)/(Z_{in} + Z_0)| \quad (2)$$

where Z_{in} is the input impedance of the absorber, Z_0 is the intrinsic impedance of free space. μ_r and ε_r are the relative complex permeability and permittivity of the absorber medium, f is the frequency of electromagnetic wave, d is the coating thickness and c is the velocity of light. The calculated results are shown in Fig. 5. It is surprising that the RL values for the pure rGO hydrogel with a thickness of 2–5 mm are more than −8 dB over 1–18 GHz. This demonstrates that pure rGO hydrogel has a very weak ability to absorb EM waves. But the EM absorption properties of the rGO/α-Fe_2O_3 composite hydrogels are significantly enhanced. It is noted that the absorption value is

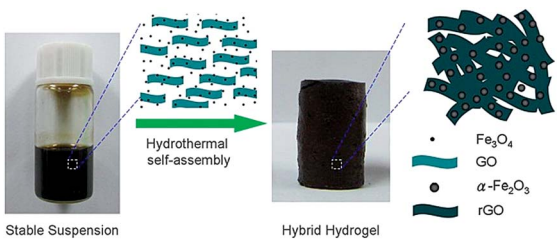

Scheme 1 Schematic illustration of the formation mechanism of the rGO/α-Fe_2O_3 composite hydrogel.

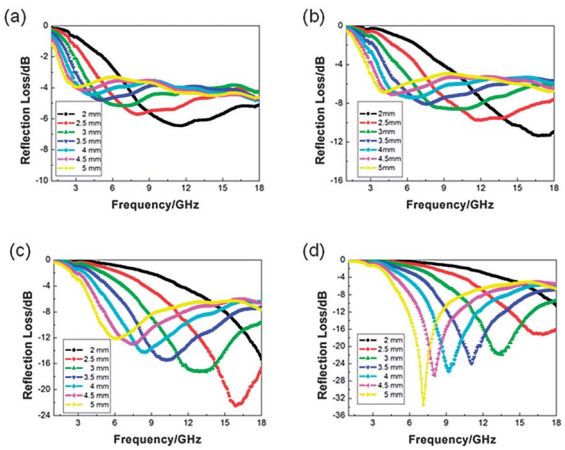

Fig. 5 Reflection loss curves for the (a) pure rGO hydrogel, the composite hydrogel with α-Fe_2O_3 weight ratios of (b) 60 wt%, (c) 76 wt% and (d) 82 wt% with different thicknesses in the frequency range of 1–18 GHz.

enhanced by increasing the weight percentage of α-Fe_2O_3. It can be seen clearly that the α-Fe_2O_3 weight ratio is 82 wt% with a coating layer thickness of 5.0 mm exhibiting a maximum absorption of −33.5 dB at 7.12 GHz. The bandwidths of RL values below −10 dB (90% of EM wave absorption) are 6.4 GHz in the range of 10.8–17.2 GHz when the sample only contains 8 wt% of the as-synthesized rGO/α-Fe_2O_3 composite hydrogel with a coating layer thickness only of 3.0 mm. Why does the rGO/α-Fe_2O_3 composite hydrogel exhibit a lower dielectric loss, but have very strong EM absorption properties? Maybe impedance match characteristics is an important concept relating to microwave absorption. Too high a permittivity of absorber is harmful to the impedance match and results in strong reflection and weak absorption.[2,13]

We also tested the EM wave absorption properties of a 2D rGO/α-Fe_2O_3 composite. The calculated RL values are shown in Fig. S2,† it can be seen that the 2D rGO/α-Fe_2O_3 composite has a weaker ability to absorb EM waves than the 3D rGO/α-Fe_2O_3 composite hydrogels (Fig. 5b) within the thickness range of 2–5 mm. This can be explained that the unique 3D porous network is another important reason for enhancing EM wave absorption properties. Therefore, the 3D rGO/α-Fe_2O_3 composite hydrogel has a great many advantages for the desire to realize practical and large-scalable applications.

Conclusions

In summary, a novel structure of a 3D rGO/α-Fe_2O_3 composite hydrogel with a prominently improved microwave absorption property has been successfully synthesized *via* a two-step process in a solution phase. The formation of α-Fe_2O_3 in the 3D framework of the rGO hydrogel greatly decreases the dielectric loss of the materials, therefore resulting in not only a wider absorption band and a larger reflection loss, but also in a lighter weight in the frequency range of 1–18 GHz. The reason may originate from the unique 3D structure and impedance match characteristics of microwave absorption. Additionally, the microwave absorption property can be tuned easily by varying the weight percentage of α-Fe_2O_3 and the layer thickness of the samples. It provides a facile method to fabricate a potential kind of good microwave absorbing material which is lightweight and has strong absorption and a wide absorption bandwidth.

Acknowledgements

This work is supported by The National Science Foundation of China (91022032, 21171001 and 21173001), the Anhui Province Key Laboratory of Environment-friendly Polymer Materials, the Science Foundation for Excellent Youth Scholars of Higher Education of Anhui Province (2012SQRL011) and the National Science Foundation of Anhui Province (1308085QB43).

Notes and references

1 A. Katsounaros, K. Z. Rajab, Y. Hao, M. Mann and W. I. Milne, *Appl. Phys. Lett.*, 2011, **98**, 203105.
2 R. C. Che, L. M. Peng, X. F. Duan, Q. Chen and X. L. Liang, *Adv. Mater.*, 2004, **16**, 401–405.
3 Q. C. Liu, J. M. Dai, Z. F. Zi, A. B. Pang, Q. Z. Liu, D. J. Wu and Y. P. Sun, *J. Low Temp. Phys.*, 2013, **170**, 261–267.
4 H.-L. Xu, H. Bi and R.-B. Yang, *J. Appl. Phys.*, 2012, **111**, 07A522.
5 K. S. Novoselov, A. K. Geim, S. V. Morozov, D. Jiang, Y. Zhang, S. V. Dubonos, I. V. Grigorieva and A. A. Firsov, *Science*, 2004, **306**, 666–669.
6 K. S. Novoselov, D. Jiang, F. Schedin, T. J. Booth, V. V. Khotkevich, S. V. Morozov and A. K. Geim, *Proc. Natl. Acad. Sci. U. S. A.*, 2005, **102**, 10451–10453.
7 H. Li, S. Pang, S. Wu, X. Feng, K. Müllen and C. Bubeck, *J. Am. Chem. Soc.*, 2011, **133**, 9423–9429.
8 Y. Xu, K. Sheng, C. Li and G. Shi, *ACS Nano*, 2010, **4**, 4324–4330.
9 P. Chen, J.-J. Yang, S.-S. Li, Z. Wang, T.-Y. Xiao, Y.-H. Qian and S.-H. Yu, *Nano Energy*, 2013, **2**, 249–256.
10 W. Chen, S. Li, C. Chen and L. Yan, *Adv. Mater.*, 2011, **23**, 5679–5683.
11 X. Huang, N. Hu, R. Gao, Y. Yu, Y. Wang, Z. Yang, E. Siu-Wai Kong, H. Wei and Y. Zhang, *J. Mater. Chem.*, 2012, **22**, 22488–22495.
12 H. Zhang, A. Xie, Y. Shen, L. Qiu and X. Tian, *Phys. Chem. Chem. Phys.*, 2012, **14**, 12757–12763.
13 C. Wang, X. Han, P. Xu, X. Zhang, Y. Du, S. Hu, J. Wang and X. Wang, *Appl. Phys. Lett.*, 2011, **98**, 072906.
14 P. F. Guan, X. F. Zhang and J. J. Guo, *Appl. Phys. Lett.*, 2012, **101**, 153108.
15 X. Bai, Y. Zhai and Y. Zhang, *J. Phys. Chem. C*, 2011, **115**, 11673–11677.
16 T. Chen, F. Deng, J. Zhu, C. Chen, G. Sun, S. Ma and X. Yang, *J. Mater. Chem.*, 2012, **22**, 15190–15197.
17 H. Yu, T. Wang, B. Wen, M. Lu, Z. Xu, C. Zhu, Y. Chen, X. Xue, C. Sun and M. Cao, *J. Mater. Chem.*, 2012, **22**, 21679–21685.
18 H.-P. Cong, X.-C. Ren, P. Wang and S.-H. Yu, *ACS Nano*, 2012, **6**, 2693–2703.
19 X.-C. Dong, H. Xu, X.-W. Wang, Y.-X. Huang, M. B. Chan-Park, H. Zhang, L.-H. Wang, W. Huang and P. Chen, *ACS Nano*, 2012, **6**, 3206–3213.
20 C. Hou, Q. Zhang, Y. Li and H. Wang, *J. Hazard. Mater.*, 2012, **205–206**, 229–235.
21 J. Li, C.-Y. Liu and Y. Liu, *J. Mater. Chem.*, 2012, **22**, 8426–8430.
22 Z.-S. Wu, S. Yang, Y. Sun, K. Parvez, X. Feng and K. Müllen, *J. Am. Chem. Soc.*, 2012, **134**, 9082–9085.
23 D. Chen, W. Wei, R. Wang, J. Zhu and L. Guo, *New J. Chem.*, 2012, **36**, 1589–1595.
24 L. Tian, Q. Zhuang, J. Li, C. Wu, Y. Shi and S. Sun, *Electrochim. Acta*, 2012, **65**, 153–158.
25 D. Wang, Y. Li, Q. Wang and T. Wang, *J. Solid State Electrochem.*, 2012, **16**, 2095–2102.
26 G.-W. Zhou, J. Wang, P. Gao, X. Yang, Y.-S. He, X.-Z. Liao, J. Yang and Z.-F. Ma, *Ind. Eng. Chem. Res.*, 2012, **52**, 1197–1204.
27 Z. Wang, C. Ma, H. Wang, Z. Liu and Z. Hao, *J. Alloys Compd.*, 2013, **552**, 486–491.

28 W. S. Hummers and R. E. Offeman, *J. Am. Chem. Soc.*, 1958, **80**, 1339.
29 Y. S. Kang, S. Risbud, J. F. Rabolt and P. Stroeve, *Chem. Mater.*, 1996, **8**, 2209–2211.
30 Y. Zhang, N. Zhang, Z.-R. Tang and Y.-J. Xu, *ACS Nano*, 2012, **6**, 9777–9789.
31 B. Ahmmad, K. Leonard, M. S. Islam, J. Kurawaki, M. Muruganandham, T. Ohkubo and Y. Kuroda, *Adv. Powder Technol.*, 2013, **24**, 160–167.
32 Y. M. Zhao, Y.-H. Li, R. Z. Ma, M. J. Roe, D. G. McCartney and Y. Q. Zhu, *Small*, 2006, **2**, 422–427.
33 Z. Liu, G. Bai, Y. Huang, Y. Ma, F. Du, F. Li, T. Guo and Y. Chen, *Carbon*, 2007, **45**, 821–827.
34 P. Xu, X. Han, C. Wang, D. Zhou, Z. Lv, A. Wen, X. Wang and B. Zhang, *J. Phys. Chem. B*, 2008, **112**, 10443–10448.
35 X. F. Zhang, X. L. Dong, H. Huang, Y. Y. Liu, W. N. Wang, X. G. Zhu, B. Lv, J. P. Lei and C. G. Lee, *Appl. Phys. Lett.*, 2006, **89**, 053115.